Article

# Experimental Study on Gas−Solid Two-Phase Flow Characteristics of a Vertical Cyclone Combustor System

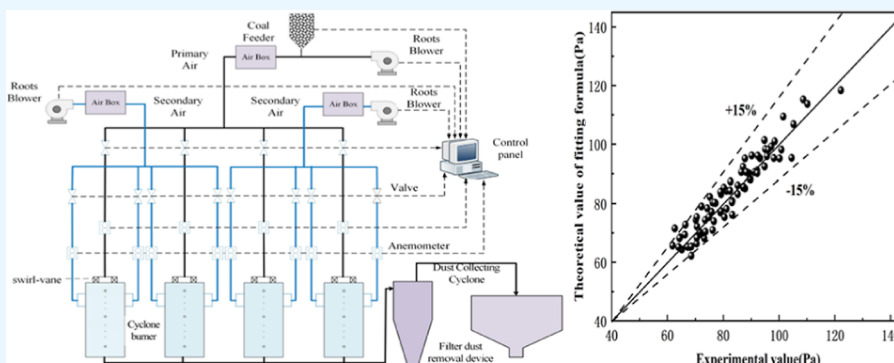Weihui Xu, Yaoyi Tang, Han Wang, Yezhu Sun, Fan Fang, Xinwei Guo, and Weishu Wang*

Read Online

ACCESS | Metrics & More | Article Recommendations

**ABSTRACT:** According to the design and operational parameters of the cyclone liquid slag-discharging boiler, an experimental platform for the cyclone burner was designed and constructed in a cold state based on the principle of similarity. The experimental study investigated the effects of parameters, such as swirl-vane angles, coal concentration, operating parameters, and particle size, on the flow distribution and vertical riser resistance characteristics of the vertical cyclone burner. The results showed that there were differences in flow distribution among the cyclone burners, and the most uniform flow distribution was achieved when the swirl-vane angle of the primary air was 30°. The concentration of pulverized coal significantly influenced the pressure drop in the vertical ascending section, which increased with higher concentrations of pulverized coal. When the concentration of pulverized coal remains constant, the pipeline pressure drop is minimized at a primary air velocity of 7.5 m/s. As the secondary wind speed increased, the pressure drop consistently rose; when the secondary wind speed is 22 m/s, the pressure drop of the pipeline is the maximum; however, excessively high secondary wind speeds were found to be detrimental to the formation of an optimal aerodynamic field in the burner. Furthermore, when the pulverized coal concentration was held constant, materials with larger particle sizes exhibited the highest pressure drop. When the particle size increases from 50 to 150 $\mu$m, the pressure drop of the vertical riser segment also increases. Finally, based on the Barth additional pressure drop theory, the pressure drop formula of the vertical riser is fitted by a dimensional analysis method, and the correlation formula of the pressure drop test of gas−solid two-phase flow in the vertical riser is obtained.

## 1. INTRODUCTION

The characteristics of China's energy and resource endowment determine that coal-fired units will continue to be the main generator units in the future for a long time. In the next 20 to 30 years, coal will maintain its dominant position in China's energy structure,[1−3] coal power plays a crucial role as a "stabilizer and ballast stone" in ensuring the stability of the nation. In light of China's commitment to the "carbon peak and carbon neutrality" objective,[4−6] China's power structure is undergoing continuous innovation, leading to an increasing proportion of installed capacity from new energy sources. Nevertheless, it is important to note that clean energy sources alone cannot provide sustainable and stable power due to various factors such as regional variations, day−night fluctuations, and climate conditions. When integrating clean

energy sources into the grid, significant impacts on the power system can occur, posing challenges when it comes to absorbing new energy.[7−9] Within the realm of coal-fired units, the boiler plays a critical role in the operational efficiency of the power station system. Particularly, coal-fired units currently in service in China have become vital for deep peak regulation. Therefore, ensuring the efficient and stable
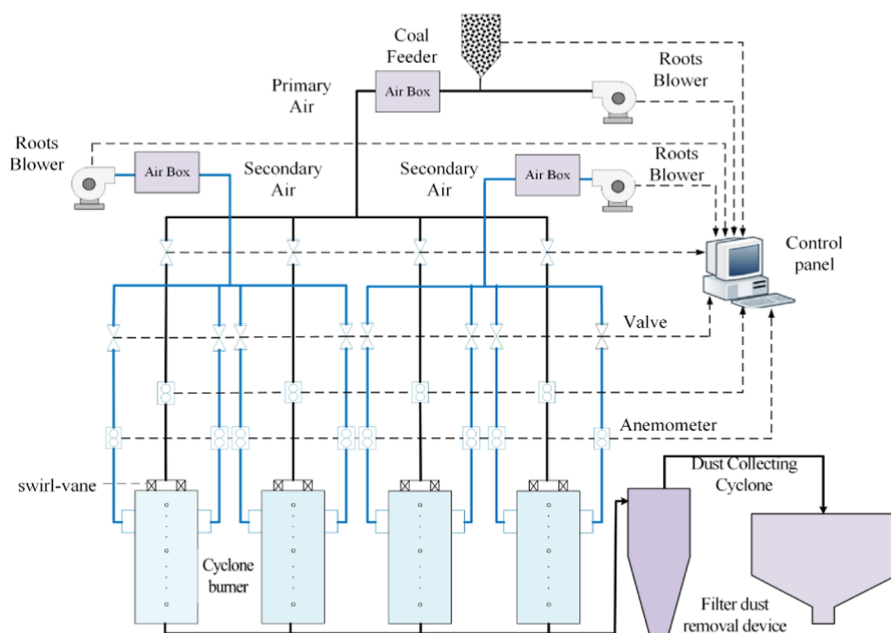
**Figure 1.** Schematic diagram of the experimental system.

operation of these units holds significant importance for the overall economy, safety, and environmental protection within the power industry.

The uniformity of air and powder flow distribution in the boiler burner system directly affects the pulverized coal combustion effect and is directly related to the economy and safety of coal-fired units. The air and powder flow distribution process of a boiler burner system is a typical gas−solid two-phase flow, and its flow characteristics are affected by structural parameters,[10] flow parameters,[11] and particle sizes.[11−13] Patro and Dash[14,15] mainly studied the effects of various parameters such as gas phase velocity and solid−gas ratio on the flow characteristics in horizontal and vertical pipes. Li et al.[16−19] used the CFD-DEM coupling method to simulate and verify the movement characteristics of pulverized coal particles in swirl pneumatic conveying processes, mainly revealing the flow characteristics, velocity distribution, and resistance characteristics of pulverized coal particles, which can provide a reference and theoretical basis for the design of pulverized coal conveying pipelines. Tang et al.[20,21] mainly studied the effects of swirl-vane angles and particle size on combustion and flow characteristics. Hirota et al.[22] studied the conveying characteristics of materials with three different densities in pipelines with varying inclinations, and it was found that density has a significant impact on the solid-phase friction coefficient. Peng and Cao[23] focused on the effect of the gas−solid phase on the gas−solid two-phase flow characteristics in the pipeline by numerical study and discussed the flow pattern in the pipeline. Deng et al.[24] conducted research on the average particle size and distribution of materials in pneumatic conveying processes. They discovered that when the size distribution range of particles is small, embolic transportation can be achieved. Yang et al.[25] utilized the coupling method of the Euler−Lagrange model and the discrete phase model to conduct numerical research on the transportation of large particles in pulverized coal. They compared their numerical results with experimental data, ultimately verifying the reliability of the model for horizontal pneumatic transportation of pulverized.

The cyclone liquid slagging boiler has characteristics of both cyclone combustion and liquid slagging, which solves the problem of only mixing high-alkali coal for power generation for a long time. The cyclone burner is an important piece of equipment of a liquid slag-discharging boiler, and its top is arranged with a cyclone blade, which can change the cyclone strength in the burner and has a great influence on the combustion in the furnace. However, research on the flow characteristics of vertical cyclone burner systems is currently limited. Many previous studies[11,20,26] have primarily concentrated on optimizing combustion in the cyclone liquid boiler furnace using numerical simulations. However, there is a dearth of experimental research on the resistance characteristics of coal transport pipelines, which calls for a more comprehensive experimental analysis. Therefore, this study aims to investigate the impact of different swirl-vane angles on the flow distribution in cyclone burners under conditions of pure air operation using cold experiments. By conducting experiments to determine the optimal swirl-vane angle, the study further examines the effects of varying feed concentration, operating parameters, and particle size on the gas−solid two-phase flow characteristics in the vertical riser section of vertical cyclone burners.

## 2. EXPERIMENTAL SYSTEM AND METHODS

**2.1. Experimental System.** Figure 1 shows a schematic diagram of the integrated cold model test platform of the cyclone burner system. The experimental system consists of five parts, namely, the air distribution system, the acquisition control system, the cyclone burner system, the feeding system, and the dust removal system. The air supply pipe and cyclone burner system are made of 10 mm transparent plexiglass, which can be visually tested. According to the layout of air supply pipes, the layout parameters of the experimental system are designed. The primary air supply pipes and secondary air supply pipes are arranged in parallel, and each pipe is equipped with an anemometer, flow-regulating valve, and differential pressure transmitter, and each device is connected by a flange. Figure 2 provides an actual diagram of the experimental

system, giving a visual representation of how the different components are arranged and connected within the platform.



**Figure 2.** Physical map of the experimental system.

Before initiating the experiment, a series of pre-experiment checks were performed. First, ensure the proper functioning of the fan and the internal software of the industrial computer. Confirm that all valves are open and verify the availability of a power supply for the test system. Additionally, check the anemometer, differential pressure transmitter, and swirl-vane angle. Once all checks are complete, we proceed with turning on the main power supply, followed by individual fan power supplies and the industrial computer with the acquisition control system.

During the pure gas phase flow characteristic test, focus on measuring the air volume in the primary air duct. To maintain a single-variable principle, we level the secondary air volume in each pipeline. This involves adjusting the primary fan and setting the initial frequency of the secondary fan. Once the airflow becomes stable, the data acquisition system is used to measure the air flow in each secondary air duct and the total air flow. Due to potential fluctuations, select an average value of at least 30 s of data and fine-tune the control valve until the air flow is balanced with a total air flow error below 1% of the test value. After fine-tuning the secondary air, minor fluctuations may occur in the primary air volume. Adjust the primary air volume to maintain a constant total primary air volume, stopping when the error is below 1%. Monitor the air volume in all secondary air ducts. Once the air volume in each pipeline stabilizes, configure the acquisition control system's settings for acquisition frequency and time to complete the experimental data measurement.

When gas−solid two-phase experiments are conducted, it is necessary to first verify the frequency of the feeding device in order to ensure the accuracy of the coal powder concentration during the experiment. First, other pipeline valves were closed, and the feeding device was adjusted to supply material to only one cyclone burner. It is required to collect test data from each pipeline for at least 60 s and calculate whether the solid-to-gas ratio meets the experimental value. Gradually adjust the experimental parameters until the error of the experimental value is within 1%. Once the airflow in each pipeline is stable, we begin collecting experimental data to complete the experiment.

**2.2. Data Processing.** During the experiment, the air volume in each pipeline will fluctuate up and down to a certain extent. In order to reduce the error in the test process, it is necessary to collect more than 2 min of data and take an average value in the process of collecting the measurement test data of the control system, and the collection frequency is 2 Hz

$$Q_i = \frac{\sum_{t=1}^{n} Q_t}{n} \tag{1}$$

where $Q_i$ and $Q_t$ are the mean and instantaneous values of branch volume flow, m$^3$/h, and $t$ is the collection time, s. $n = 4$, where $n$ represents four parallel pipelines of the experimental system.

The mass flow rate of the material in the primary air duct is an instantaneous value, but when the working conditions remain unchanged and after a period of full development, the mass flow rate of the solid phase is basically unchanged. The mass flow rate $M_s$ in this paper refers to the average value, which can be calculated by Formula 2

$$M_s = 3600 \frac{W_2 - W_1}{t_2 - t_1} \tag{2}$$

In the formula, the unit of $M_s$ is kg/s and $W_2$ and $W_1$ correspond to the amount of powder in the feeding device at $t_2$ and $t_1$, respectively. The units of $W_1$ and $W_2$ are kg and the units of $t_2$ and $t_1$ are seconds.

$\mu$ is expressed as the ratio of solid-to-gas, as shown in (3) below

$$\mu = \frac{M_s}{Q \cdot \rho_g} \tag{3}$$

where $Q$ is the volume flow rate of the gas and $\rho_g$ is the density of the gas.

In order to characterize the stability of the transportation process, the fluctuation of the instantaneous pressure drop can well reflect the stability of the transportation process. CVs is the sum of the standard deviation coefficient CV of each working condition under the corresponding wind speed, and the sum of the standard deviation coefficient CV and the standard deviation coefficient CV of each working condition is calculated according to Formulas 4 and 5

$$CV = \frac{\text{standard deviation of pressure drop}}{\text{average pressure drop}} \tag{4}$$

$$CV_s = \sum_{i=1}^{n} CV_i \tag{5}$$

Research working condition range: swirl-vane angles: 25−45°; primary wind speed: 6−10 m/s; and secondary wind speed: 12.25−20.25 m/s.

## 3. EXPERIMENTAL RESULTS AND ANALYSIS

**3.1. Influence of Swirl-Vane Angle on Flow Distribution.** Figure 3 illustrates the impact of swirl-vane angle changes on the flow distribution characteristics of each cyclone burner, and the primary wind speed ranges from 6 to 10 m/s. The flow rate of no. 1 to no. 4 burners exhibits a decreasing trend, in which the flow deviation of no. 1 and no. 4 burners is the largest. This is because the pipeline layout is different, and the uneven flow distribution is mainly affected by the resistance along the flow. The resistance of the four primary air branches is different along the way, and the resistance increases successively from branch 1 to branch 4. The significant disparity in resistance between the first and fourth branches results in the most uneven air volume distribution between the corresponding no. 1 and no. 4 burners. As Figure 4 shows, with the increase of swirl-vane angle, the air volume distributed by
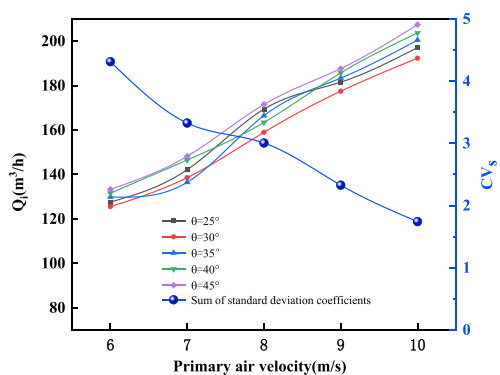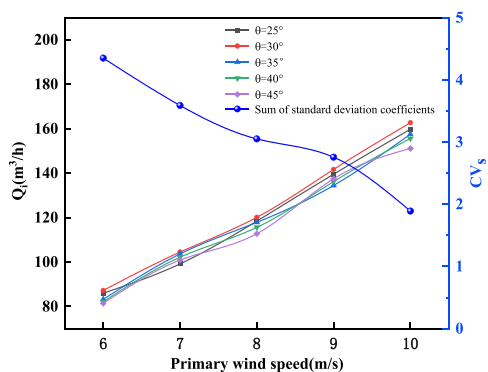
(a) Burner # 1
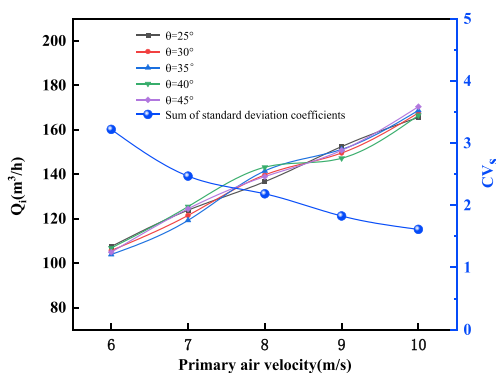


(b) Burner # 2
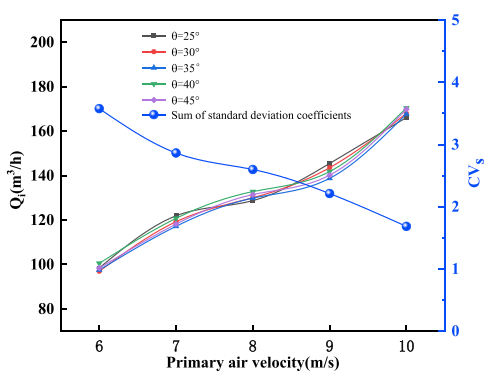


(c) Burner # 3



(d) Burner # 4

**Figure 3.** Influence of swirl-vane angle change on flow distribution of each burner when $V_2 = 18.15$ m/s.
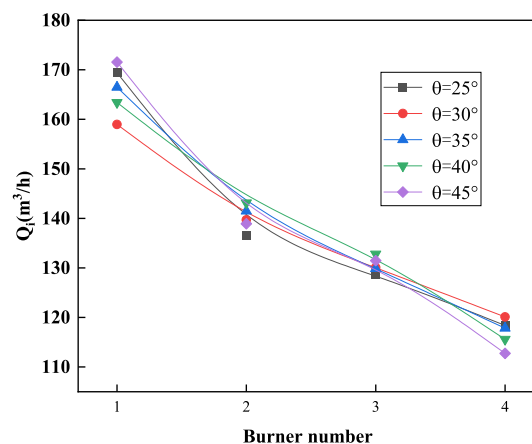


**Figure 4.** Influence of swirl-vane angle change on flow distribution of each burner when $V_1 = 8$ m/s.

burner no. 1 first decreases and then increases, while that of burner no. 4 increases at first and then decreases. This is because when the swirl-vane angle increases to 30°, the flow area of the primary air inlet area decreases. As a result, there is an increase in local resistance in that particular area. Additionally, the air velocity at the inlet of burner no. 1 was higher than that of burner no. 4, resulting in a higher proportionate increase in local resistance for branch 1 compared to branch 4. This generated a larger contribution to the overall resistance from local resistance, weakening the impact of resistance along the path on the flow distribution within the entire system. At this time, the influence of the local resistance on the flow distribution is greater than that of the resistance along the way and the uniformity of the flow distribution is improved. However, when the swirl-vane angle increases to more than 30°, the influence of local resistance on flow distribution becomes the predominant factor, and further increasing the swirl-vane angle does not promote better uniformity of flow distribution among the burners. Therefore, 30° is selected as the optimal swirl-vane angle in the study working condition range.

With the increase in primary wind speed, the $CV_s$ of each burner exhibits a decreasing trend. $CV_s$ is an important index to characterize the stability of the transportation process. The larger the $CV_s$, the greater the sum of deviations between the instantaneous pressure drop of nodes at each time during the transportation process and the average pressure drop during the transportation process under various working conditions, and the worse the transportation stability. Under each working condition, the $CV_s$ of no. 1 and no. 4 burners is higher, the $CV_s$ of no. 3 burner is lower, and the $CV_s$ of no. 2 burner is the lowest. The reason behind these observations is that the air volume of burner no. 1 is the largest under each working condition, resulting in the highest flow fluctuation and the poorest conveying stability. On the other hand, burner no. 2 experiences the smallest flow fluctuation under each working condition, indicating the most stable transmission.

**3.2. Influence of Pulverized Coal Concentration on Pipeline Resistance Characteristics.** Figure 5 shows the influence of the pulverized coal concentration on pipeline resistance characteristics when the primary wind speed is 6−10 m/s. It can be seen from the figure that the pressure drop in the vertical rising section changes with the primary wind speed similarly under different coal powder concentrations. At the
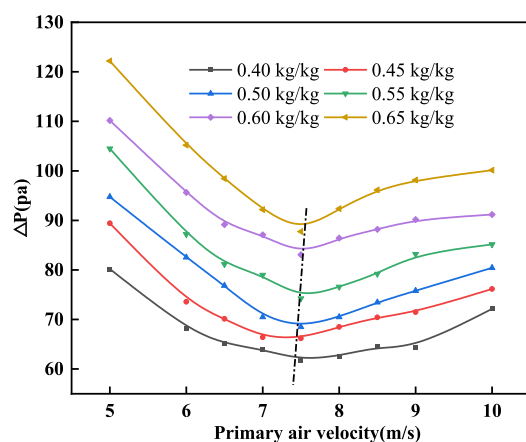
**Figure 5.** Influence of pulverized coal concentration on pipeline resistance characteristics when $V_2 = 18.15$ m/s.



**Figure 6.** Influence of different secondary wind speeds on pipe resistance characteristics.

same primary wind speed, the pressure drop initially decreases and then increases with the increase of pulverized coal concentration. This behavior is attributed to the two main components of pipeline pressure loss: gas phase pressure loss and solid phase pressure loss. Under the same concentration of pulverized coal, an increase in primary wind speed leads to an increase in friction loss between the gas flow and the pipe wall, as well as between the gas phase and the solid phase. Consequently, the gas phase pressure loss within the pipeline increases. Similarly, at the same pulverized coal concentration, the proportion of gas phase mass flow increases with the increase of primary wind speed. This results in a dilution of the solid−gas ratio and a reduction in the pressure loss of the solid phase. Additionally, at low primary wind speeds, the proportion of solid pressure drop is much larger than that of gas pressure loss. However, when the primary wind speed increases, the minimum value of pipeline pressure drop will appear under the corresponding primary wind speed. The optimal economic gas speed, in this case, is observed when the primary wind speed is 7.5 m/s.

It can also be seen from the figure that with the increase of pulverized coal concentration, the pressure drop will be higher, and the mass flow rate will also rise with the increase of pulverized coal concentration, which will lead to more intense collisions and friction between particles so the pressure drop in the vertical riser section will increase.

**3.3. Influence of Different Operating Parameters on Pipeline Resistance Characteristics.** Figure 6 shows the influence of different secondary wind speeds on the resistance characteristics of the pipeline when the concentration of pulverized coal is 0.55 kg/kg. The figure reveals that with an increase in secondary wind speed, the pressure drop also increases under each operating condition. This phenomenon can be attributed to the elevated disturbance caused by the higher secondary wind speed at the axial entry of the primary wind, leading to increased local resistance in the area of the cyclone burner inlet. When the primary wind speed is 6 m/s, the axial component of the primary wind gas is relatively low. Under this condition, the gas's ability to carry powder is weakened. In this scenario, some particles may slightly exceed the suspension speed, leading to their movement within the vertical riser tube. This movement intensifies the collision between particles as well as between particles and the wall surface, subsequently increasing the friction-induced pressure
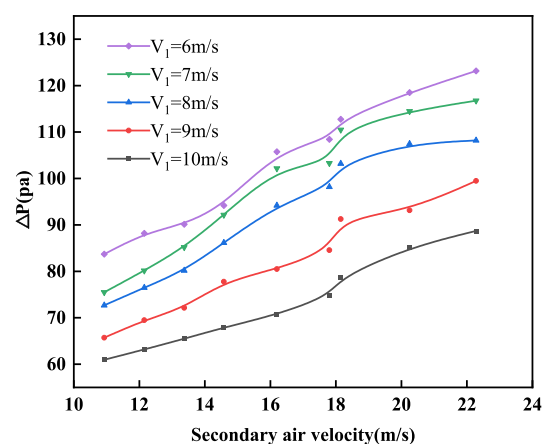
drop in the solid phase. Consequently, the total pressure drop rises.

Furthermore, under conditions of low gas velocity, the pressure drop in the pipeline primarily depends on the pressure drop in the solid phase. It is worth noting that the particle phase concentration is higher when the primary wind speed is low. The friction-induced pressure drop in the solid phase is closely associated with the drag force between the gas and the solid. Therefore, excessively high secondary air concentrations are not conducive to establishing a favorable aerodynamic field within the burner.

**3.4. Influence of Different Particle Sizes on Pipeline Resistance Characteristics.** Figure 7 illustrates the impact of
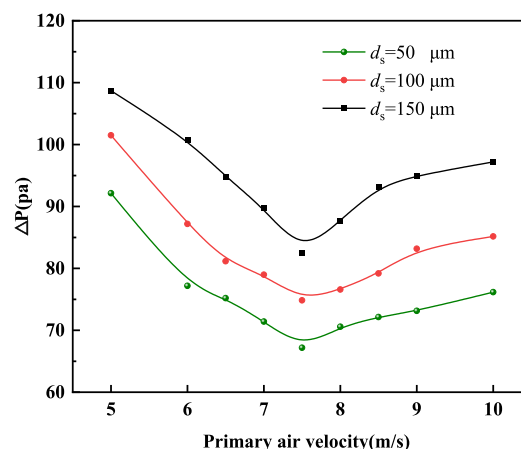


**Figure 7.** Influence of particle size on pipe resistance characteristics.

particle size on pipe resistance characteristics at a pulverized coal concentration of 0.55 kg/kg. The results reveal that under constant pulverized coal concentration, the pressure drop in the vertical ascending section of the pipeline exhibits an initial decrease followed by an increase with increasing primary wind speed. Furthermore, as the particle size increases, the pressure drop experienced in the vertical ascending pipe section also increases. This can be attributed to the greater gravitational force exerted on the larger particles. The suspension speed denotes the minimum velocity required to maintain particle suspension; beyond this threshold, particles ascend. Notably, the suspension speed is directly proportional to the square root of the particle size ($d_s$), indicating that particles with larger

sizes have higher suspension speeds. Consequently, particles with larger sizes exhibit enhanced upward movement due to higher suspension speeds, leading to increased collisions and frictional effects. As a result, the pressure drop in the vertical ascending pipe section is greater for the larger particles.

Furthermore, the followability of powder with a large particle size with primary air flow is worse than that of powder with a small particle size. Conversely, when the particle size ($d_s$) increases from 50 to 150 $\mu$m, the pressure drop in the vertical riser section is also higher. This is because particles with large suspension velocity are more likely to settle to the bottom of the pipeline, thereby reducing the flow area of the pipeline in a different phase, which leads to increased friction and collision between particles and the pipe wall and increased friction loss.

**3.5. Pressure Drop Formula Fitting Results and Analysis.** *3.5.1. Additional Pressure Drop Method.* The additional pressure drop method is a widely used calculation method of pipeline pressure drop, which was originally derived by Barth[27] based on the energy theory. After the two-phase flow is fully developed, it can be simplified as Formula 6

$$\Delta P_t = \Delta P_g + \Delta P_s \tag{6}$$

In the formula, $\Delta P_g$ represents the gas phase pressure drop in the stable section and $\Delta P_s$ represents the solid phase pressure drop in the stable section.

For the gas phase pressure drop $\Delta P_g$ in the stable section, many theories have been studied at home and abroad and are very mature. $\Delta P_g$ can be calculated according to Formula 7

$$\Delta P_g = \lambda_g \rho_g \frac{U^2}{2} \tag{7}$$

where $U$ is the volume flow in the pipeline divided by the cross-sectional area, that is, the primary wind speed and $\lambda_g$ is the gas phase pressure drop coefficient, which can be calculated according to Formula 8

$$\lambda_g = 0.079 Re^{-0.25} \tag{8}$$

where $Re$ is Reynolds number and $\rho_g$ is gas density kg/m$^3$, in the actual process, the flow inside the pipeline is more complex, and the velocity of the solid phase is generally difficult to measure by existing means, therefore, Formula 9 is generally adopted

$$\Delta P_s = \frac{\lambda_s \mu \rho_g u_g^2 L}{2D} \tag{9}$$

where $D$ represents the internal diameter of the pipeline, mm, and $L$ represents the pipe length, m. $\lambda_s$ represents the solid phase pressure drop coefficient and $u_g$ represents the gas phase velocity. $\mu$ is expressed as the ratio of the solid-to-gas.

*3.5.2. Pressure Drop Correlation.* The gas−solid, two-phase flow process is affected by many factors. Scholars used a large number of test and simulation data to fit the pressure drop correlation formula. However, the application range of different correlation formulas is relatively limited, and there is no universal correlation formula that can adapt to all working conditions. Geldart[28] believes that the horizontal pipe pressure drop transport under high pressure in the horizontal pipe can be shown in the following Formula 10

$$\frac{\Delta P}{L} = \frac{0.83 \left(\frac{G_s}{D}\right)^{1.28} \left(\frac{\mu_g}{\rho_g}\right)^{0.4}}{U} \tag{10}$$

where $G_s$ denotes the solid mass flux of solids, [kg/ (m$^2$/s)]. $\mu_g$ represents gas viscosity, kg/(m s).

To accurately account for the vertical riser pressure drop, eq 10 should be considered along with the influence of the material's gravity itself. This can be represented by Formula 11, as shown below

$$\frac{\Delta P}{L} = \frac{0.83 \left(\frac{G_s}{D}\right)^{1.28} \left(\frac{\mu_g}{\rho_g}\right)^{0.4}}{U} + \rho_s g H (1 - \varepsilon) \tag{11}$$

where $H$ represents the vertical distance between the powder discharge point and the feed point, m; $g$ represents gravitational acceleration and 9.81 m/s$^2$; and $\varepsilon$ represents the volume ratio of particles. According to Formula 11, the vertical tube pressure drop under experimental conditions in this paper is calculated, and the comparison is shown in Figure 8.
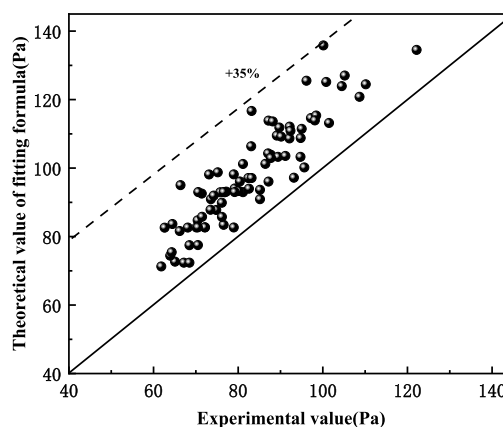


**Figure 8.** Comparison of predicted values and experimental values of the Geldart empirical formula for the vertical riser tube.

As can be seen from Figure 8, the predicted values of the Geldart formula are all higher than the experimental values, and the maximum error is about 35%. The main reason is that the pressure of the Geldart experimental conditions is higher than that of the research conditions in this paper. As the pressure increases, the interaction force between the gas and solid phases will also increase, and the interaction force between the particles and the pipe wall will also increase, resulting in the pressure drop, as calculated by the formula, being higher than the actual experimental value.

Generally speaking, the pressure drop of gas−solid two-phase flow in the pipeline is related to the concentration of pulverized coal, the apparent gas velocity, the average particle size of the material, and the operating parameters. For vertical riser tubes, the additional coefficient of pressure drop can be written in the form of Formula 12

$$\lambda_s = f(\mu, U, D, g, \rho_g, \rho_s, d_s) \tag{12}$$

where $\rho_g$ and $\rho_s$ represent the gas density and particle density, respectively, kg/m$^3$. The $\pi$ theorem can be rewritten into the following functional relationship using dimensional analysis

$$\lambda_s = \phi Fr^m \mu^n \left(\frac{\rho_s}{\rho_g}\right)^p \left(\frac{d_s}{D}\right)^q \tag{13}$$

where $Fr$ stands for the Froude number in the formula. Since the object of study is a vertical riser, the Froude number related to gravity is the focus of consideration. In the $\lambda_s$ correlation, $\phi$, $m$, $n$, $p$, and $q$ are all undetermined formula coefficients. Regression analysis was carried out on multiple groups of test data, and the undetermined coefficients after fitting are shown in Table 1.

**Table 1. Fitting Results of Empirical Formula Coefficients**

| undetermined coefficient | ø | m | n | p | q |
|---|---|---|---|---|---|
| fitting result | −7.891 | −15.36 | 1.54 | 4.073 | 6.11 |

By bringing the obtained undetermined experience coefficient into the functional correlation formula, the solid phase additional coefficient of vertical riser pressure drop is obtained as follows

$$\lambda_s = e^{-7.891} Fr^{-15.36} \mu^{1.54} \left(\frac{\rho_s}{\rho_g}\right)^{4.073} \left(\frac{d_s}{D}\right)^{6.11} \tag{14}$$

where $e$ is a dimensionless number. The formula of riser pressure drop obtained by simultaneous Formulas 6−9 is as follows

$$\Delta P = 0.079 Re^{-0.25} \frac{L}{D} \rho_g \frac{v_g^2}{2} + e^{-7.891} Fr^{-15.36} \mu^{1.54} \left(\frac{\rho_s}{\rho_g}\right)^{4.073}$$
$$\left(\frac{d_s}{D}\right)^{6.11} \mu \rho_g \mu_g^2 L/(2D) \tag{15}$$

The comparison between the calculated value of the fitting formula and the experimental results of the vertical riser pressure drop is shown in Figure 9. The obtained pressure drop formula is more accurate for the prediction of vertical riser in this paper, the goodness-of-fit coefficient ($R^2$) is determined to be 0.948, and the relative error is found to be less than 15%. These results provide a solid theoretical foundation and support for the pipeline design of coal-fired units.
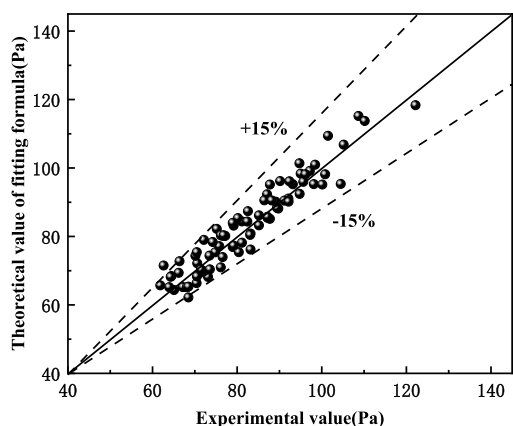


**Figure 9.** Comparison between the predicted value of the pressure drop fitting formula and the experimental results.

## 4. CONCLUSIONS

In this paper, the resistance characteristics of the vertical cyclone burner system are investigated under cold conditions. First, an integrated cold model test platform of cyclone burners based on the principle of similar modeling is introduced. Next, the distribution of burner flow rates under rated parameters is investigated, and the impact of swirl-vane angles on the flow distribution characteristics of the cyclone burner under gas phase operating conditions is explored. Building upon this, the effects of the coal powder concentration, operating parameters, and particle size on the resistance characteristics of the cyclone burner are analyzed. Finally, based on the experimental research and theoretical analysis, a fitting formula for the vertical pipe pressure drop is derived. The following conclusions are drawn:

1 There are significant differences in the flow distribution among the burners, which are influenced by the arrangement of the pipelines. The flow rates allocated to burners 1 to 4 decrease sequentially. Excessive swirl-vane angles increase local resistance at the entrance of the cyclone burner, resulting in further reductions in flow distribution uniformity. When the swirl-vane angle is 30°, the flow distribution of each burner is the most uniform.

2 Under different pulverized coal concentrations, the pressure drop in the vertical ascending section changes similarly with the primary wind speed. Under the same primary wind speed, with the increase of pulverized coal concentration, the pressure drop first decreases and then increases; with the increase of primary wind speed, the transport stability increases; under the same pulverized coal concentration, the pressure drop increases with the increase of secondary wind speed, and the high secondary wind speed will reduce the conveying stability. Under the same pulverized coal concentration, the pipe pressure drop in the vertical ascending section decreases first and then increases with the increase of primary wind speed. Furthermore, as the particle size increases, the pressure drop in the vertical ascending section also increases. The conveying stability of particles with larger sizes is found to be lower compared to that of smaller particles.

3 Based on the Barth additional pressure drop theory, the pressure drop formula for the vertical riser was derived using the dimensional analysis method. This formula was then compared to the Geldart pressure drop formula. Notably, the comparison revealed that the predicted values from the Geldart formula were overestimated due to variations in the experimental conditions. As a result, an empirical correlation equation for the pressure drop of gas−solid two-phase flow in the vertical riser was obtained through experimental testing. This correlated equation provides a more accurate estimation for the pressure drop in the vertical riser under the specific experimental conditions studied.

## ■ AUTHOR INFORMATION

**Corresponding Author**

**Weishu Wang** − *School of Electric Power, North China University of Water Resources and Electric Power, Henan 450045, China;* ⊙ orcid.org/0000-0001-7623-4047;

Phone: +86-13733870955; Email: wangweishu@ncwu.edu.cn; Fax: +86-0371-65790043

## Authors

**Weihui Xu** − *School of Electric Power, North China University of Water Resources and Electric Power, Henan 450045, China*

**Yaoyi Tang** − *School of Electric Power, North China University of Water Resources and Electric Power, Henan 450045, China;* orcid.org/0009-0007-3404-6647

**Han Wang** − *School of Electric Power, North China University of Water Resources and Electric Power, Henan 450045, China*

**Yezhu Sun** − *Huaneng Power International, Beijing 100031, China*

**Fan Fang** − *Huaneng Xi'an Thermal Engineering Research Institute, Xian 710032, China*

**Xinwei Guo** − *School of Electric Power, North China University of Water Resources and Electric Power, Henan 450045, China;* orcid.org/0000-0002-3626-947X

Complete contact information is available at:
https://pubs.acs.org/10.1021/acsomega.3c06656

## Notes

The authors declare no competing financial interest.

## ■ REFERENCES

(1) Xue, L.; Zhang, W.; Zheng, Z.; Liu, Z.; Meng, S.; Li, H.; Du, Y. Measurement and influential factors of the efficiency of coal resources of China's provinces: Based on Bootstrap-DEA and Tobit. *Energy* **2021**, *221*, 119763.

(2) Li, C.; Nie, R. An evaluating system for scientific mining of China's coal resources. *Resour. Pol.* **2017**, *53*, 317−327.

(3) Hu, Z.; Yang, G.; Xiao, W.; Li, J.; Yang, Y.; Yu, Y. Farmland damage and its impact on the overlapped areas of cropland and coal resources in the eastern plains of China. *Resour. Conserv. Recycl.* **2014**, *86*, 1−8.

(4) Pingjian, Y.; Shuan, P.; Nihed, B.; et al. An integrated evaluation on China's provincial carbon peak and carbon neutrality. *J. Clean. Prod.* **2022**, *377*, 134497.

(5) Wang, Y.; Guo, C.; Chen, X.; et al. Carbon peak and carbon neutrality in China: Goals, implementation path and prospects. *Chin. Geol.* **2021**, *4* (04), 720−746.

(6) Liu, L.; Guo, H.; Dai, L.; Liu, M.; Xiao, Y.; Cong, T.; Gu, H. The role of nuclear energy in the carbon neutrality goal. *Prog. Nucl. Energy* **2023**, *162*, 104772.

(7) Li, X.; Pan, L.; Zhang, J. Development status evaluation and path analysis of regional clean energy power generation in China. *Energy Strategy Rev.* **2023**, *49*, 101139.

(8) Raghutla, C.; Chittedi, K. R. The effect of technological innovation and clean energy consumption on carbon neutrality in top clean energy-consuming countries: A panel estimation. *Energy Strategy Rev.* **2023**, *47*, 101091.

(9) Chen, P.; Dagestani, A. A. Urban planning policy and clean energy development Harmony-evidence from smart city pilot policy in China. *Renew. Energy* **2023**, *210*, 251−257.

(10) Yang, D.; Xing, B.; Li, J.; Wang, Y.; Gao, K.; Zhou, F.; Xia, Y.; Wang, C. Experimental study on the injection performance of the gas-solid injector for large coal particles. *Powder Technol.* **2020**, *364*, 879−888.

(11) Zhu, T.; T.ang, C.; Ning, X.; Wang, L.; Deng, L.; Che, D. Experimental study on $NO_x$ emission characteristics of Zhundong coal in cyclone furnace[J]. *Fuel* **2022**, *311*, 122536.

(12) Li, J.; Zhou, F.; Yang, D.; Yu, B.; Li, Y. Effect of swirling flow on large coal particle pneumatic conveying. *Powder Technol.* **2020**, *362* (C), 745−758.

(13) Zhou, F.; Hu, S.; Liu, Y.; Liu, C.; Xia, T. CFD−DEM simulation of the pneumatic conveying of fine particles through a horizontal slit. *Particuology* **2014**, *16*, 196−205.

(14) Patro, P.; Dash, S. K. Two-fluid modeling of turbulent particle−gas suspensions in vertical pipes. *Powder Technol.* **2014**, *264*, 320−331.

(15) Patro, P.; Dash, S. K. Numerical Simulation for Hydrodynamic Analysis and Pressure Drop Prediction in Horizontal Gas-Solid Flows. *Part. Sci. Technol.* **2014**, *32* (1), 94−103.

(16) Li, K.; Kuang, S.; Pan, R.; Yu, A. Numerical study of horizontal pneumatic conveying: Effect of material properties. *Powder Technol.* **2014**, *251* (1), 15−24.

(17) Zhou, J.; Liu, Y.; Du, C.; Liu, S. y. Effect of the particle shape and swirling intensity on the breakage of lump coal particle in pneumatic conveying. *Powder Technol.* **2017**, *317*, 438−448.

(18) Zhou, J.; Du, C. l.; Ma, Z. Influence of swirling intensity on lump coal particle pickup velocity in pneumatic conveying. *Powder Technol.* **2018**, *339*, 470−478.

(19) Zhou, J.; Liu, Y.; Du, C.; Liu, S.; Li, J. Numerical study of coarse coal particle breakage in pneumatic conveying. *Particuology* **2018**, *38* (3), 204−214.

(20) Tang, C.; Zhu, T.; Hu, Y.; Wang, L.; Che, D.; Liu, Y. Numerical Investigation of the Effects of Swirl-Vane Angle and Particle Size on Combustion and Flow Characteristics in a Vertical Cyclone Barrel. *J. Energy Eng.* **2020**, *146* (4), 04020029.

(21) Xi, Z.; Liu, Z.; Shi, X.; Lian, T.; Li, Y. Numerical investigation on flow characteristics and emissions under varying swirler vane angle in a lean premixed combustor. *Case Stud. Therm. Eng.* **2022**, *31*, 101800.

(22) Hirota, M.; Sogo, Y.; Marutani, T.; Suzuki, M. Effect of mechanical properties of powder on pneumatic conveying in inclined pipe. *Powder Technol.* **2002**, *122* (2−3), 150−155.

(23) Peng, W.; Cao, X. Numerical prediction of erosion distributions and solid particle trajectories in elbows for gas−solid flow. *J. Nat. Gas Sci. Eng.* **2016**, *30*, 455−470.

(24) Deng, T.; Bradley, M. S. A. Determination of a particle size distribution criterion for predicting dense phase pneumatic conveying behaviour of granular and powder materials. *Powder Technol.* **2016**, *304*, 32−40.

(25) Yang, D.; Li, G.; Wang, Y.; et al. Prediction of horizontal pneumatic conveying of large coal particles using discrete phase model. *Adv. Mater. Sci. Eng.* **2020**, *2020*, 1967052.

(26) Wang, W.; Sun, Y.; Huang, Z.; Liao, Y.; Fang, F. Numerical Simulation of $NO_x$ Emission Characteristics of a Cyclone Boiler with Slag-Tap Furnace[J]. *ACS Omega* **2020**, *5* (46), 29978−29987.

(27) Barth, W. Strömungsvorgänge beim Transport von Festteilchen und Flüssigkeitsteilchen in Gasen. mit besonderer Berücksichtigung der Vorgänge bei pneumatischer Förderung. *Chem. Ing. Tech.* **1958**, *30* (3), 171−180.

(28) Geldart, D.; Ling, S. J. Dense phase conveying of fine coal at high total pressures. *Powder Technol.* **1990**, *62* (3), 243−252.